Semiclassical calculation of bound states in multidimensional systems with Fermi resonance

D. W. Noid

Oak Ridge National Laboratory, Oak Ridge, Tennessee 37830

M. L. Koszykowski

Sandia Laboratories, Livermore, California 94550

R. A. Marcus

Arthur Amos Noyes Laboratory of Chemical Physics, California Institute of Technology,[a] *Pasadena, California 91125*

A method is devised to calculate eigenvalues semiclassically for an anharmonic system whose two unperturbed modes are 2:1 degenerate. For some special states the periodic energy exchange between unperturbed modes is found to be very large. The quantum mechanical wave functions are examined and a correlation with the classical trajectories is described, both for quasiperiodic and the stochastic cases. A method used in the literature for calculating the stochastic limit is tested and found to break down when the present anharmonic system is separable.

I. INTRODUCTION

The phenomenon of Fermi resonance[1] is a well-known example of resonant coupling between two degrees of freedom in a molecular system, occurring when two oscillators have a frequency ratio of 2:1. For example, in CO_2 one stretching frequency of 1337 cm^{-1} is almost twice the bending frequency of 667 cm^{-1}. A dynamic interaction causes a splitting of the degeneracy, yielding instead of a 1337 cm^{-1} Raman line, two lines, one at 1388 cm^{-1} and the other at 1286 cm^{-1}. Fermi resonances also occur in many other molecules.

In earlier papers of the present series, eigenvalues were calculated semiclassically using the classical trajectories of systems of two oscillators for both nondegenerate[2-4] and 1:1 degenerate systems.[5] Good agreement was found with the quantum results. Other semiclassical methods have also recently been developed,[6] although only surface of section methods have been applied to systems with zeroth order degeneracy.[5, 6b]

The 1:1 degenerate case has an element not present in the nondegenerate one, namely the existence of two types of quasiperiodic trajectories—librating and precessing, and a transition between them.[5] The change in caustic structure during this transition involved the coalescence of some caustics and the formation of new ones. This change was examined in some detail in order to understand the nature of the semiclassical quantum conditions for such systems.[5]

The present degenerate case for $\omega_x : \omega_y = 2:1$ is seen below to have three types of trajectories, one serving as a transitional type between the other two. The semiclassical formalism is developed in the present paper to treat the three types, and the eigenvalues are calculated and compared with the quantum ones.

The specific form of the Hamiltonian employed is the same as in previous papers of this series:

$$H = \tfrac{1}{2}(p_x^2 + p_y^2 + \omega_x^2 x^2 + \omega_y^2 y^2) + \lambda x(y^2 - \alpha x^2) , \qquad (1.1)$$

where ω_x and ω_y were incommensurate in Refs. 3 and 4, 1:1 in Ref. 5, and 2:1 in the present paper. The case where $\omega_x : \omega_y = 1:2$ is also described here.

II. UNPERTURBED SYSTEM AND QUANTIZATION

The unperturbed Hamiltonian is

$$H_0 = \tfrac{1}{2}(p_x^2 + p_y^2 + \omega_x^2 x^2 + \omega_y^2 y^2) . \qquad (2.1)$$

When ω_x and ω_y are incommensurate, the single trajectory for (2.1) with given action variables[7] (J_x, J_y) sweeps out a region covered by a rectangular box (cf. Fig. 1, Ref. 2). Small perturbations of such a system led only to small distortions of the box (cf. Fig. 1, Ref. 4).

When resonances arise, namely when

$$n_x \omega_x - n_y \omega_y = 0 , \qquad (2.2)$$

where n_x and n_y are small positive integers, a major distortion of the region swept out can occur, e.g., as in the case of a 1:1 resonance for the case $\alpha = 1/3$,[5] where the region swept out by a perturbed precessing trajectory became an annulus instead of a box. Polar coordinates and their related action variables were used in discussing the behavior and making a semiclassical quantization.[5] The unperturbed Hamiltonian (2.1) was separable in Cartesian coordinates and, when $\omega_x = \omega_y$, also in polar coordinates.

When ω_x/ω_y equals 2 or 1/2, the unperturbed Hamiltonian (2.1) is separable both in Cartesian and parabolic coordinates. Each unperturbed trajectory is a closed figure-eight. An ensemble of them for given values of the Cartesian action variables (J_x, J_y) fills up a rectangular box in (x, y) space. The perturbed Hamiltonian (1.1) contains terms such as $\sin 2\pi(w_x + 2w_y)$, $\sin 2\pi(w_x - 2w_y)$, and $\sin 2\pi w_x$ (Appendix A). (The w's are angle variations conjugate to J_x and J_y.) When $\omega_x = 2\omega_y$, the perturbation term $\sin 2\pi(w_x - 2w_y)$ is a "secular" perturbation.[7] The

shape of the region swept out is thereby very different from a box, and will be seen from figures given later to be a parabolic-shaped region. Thus, to quantize such trajectories semiclassically we consider instead the results of initial separation of variables in (2.1) in parabolic coordinates, ξ and η. In contrast, the $\omega_y = 2\omega_x$ unperturbed system is also separable in parabolic coordinates, but now the $\sin2\pi(w_x - 2w_y)$ does not act as a secular perturbation for this system, and for this system a perturbed trajectory sweeps out a boxlike region instead of a parabolic one. In resonances other than $1:1$, secular terms are at least sometimes needed for the perturbed trajectory (when polynomials are the perturbation) to cover a region in (x, y) space other than a box-shaped one.

In terms of the parabolic coordinates ξ and η the Cartesian coordinates x and y are given by[8]

$$x = (\xi^2 - \eta^2)/2 \ , \quad y = \xi\eta \ , \tag{2.3}$$

and the unperturbed Hamiltonian (2.1) is given by (2.4) upon setting $\omega_x = 2$ and $\omega_y = 1$,

$$H_0 = (p_\xi^2 + p_\eta^2 + \xi^6 + \eta^6)/2(\xi^2 + \eta^2) \ . \tag{2.4}$$

To obtain the Hamilton–Jacobi equation corresponding to (2.4), p_ξ and p_η are replaced by $\partial S/\partial\xi$ and $\partial S/\partial\eta$, respectively, where S is a function to be determined, and H_0 is set equal to E. A separation of variables is introduced by setting

$$S(\xi, \eta) = S_1(\xi) + S_2(\eta) \ . \tag{2.5}$$
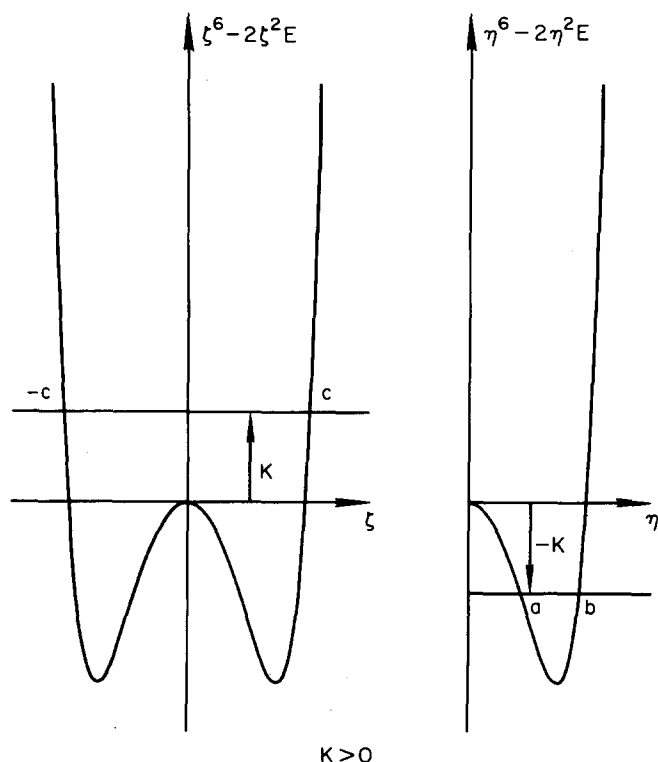
One obtains, after rearranging the terms,

FIG. 1. Plots of an effective potential $\xi^6 - 2\eta^2 E$ [cf. Eq. (2.7)] and of $\eta^6 - 2\pi^2 E$ [cf. Eq. (2.8)] for the case $K > 0$. p_ξ^2 and p_η^2 and given by Eqs. (2.7) and (2.8).
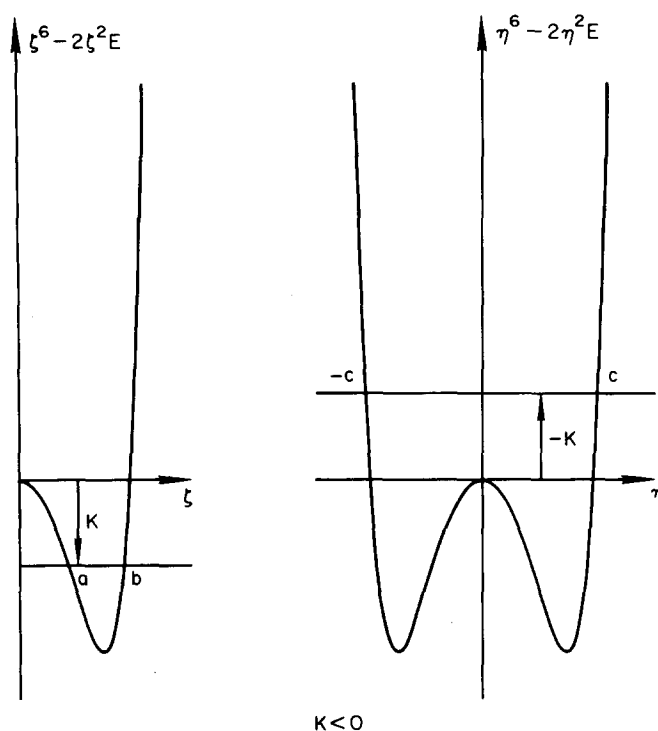

FIG. 2. Plots similar to Fig. 2 but for $K < 0$.

$$(dS_1/d\xi)^2 + \xi^6 - 2\xi^2E = - [(dS_2/d\eta)^2 + \eta^6 - 2\eta^2E] \ , \tag{2.6}$$

noting thereby that both sides of (2.6) are independent of ξ and η and so can be set equal to some constant K. One obtains

$$p_\xi^2 + \xi^6 - 2\xi^2E = K \tag{2.7}$$

$$p_\eta^2 + \eta^6 - 2\eta^2E = -K \ . \tag{2.8}$$

In Fig. 1 for $K > 0$ are given plots of $\xi^6 - 2\xi^2E$ versus ξ and $\eta^6 - 2\eta^2E$ versus η. In this coordinate system the transformation is not $1:1$ if the signs of both ξ and η are unrestricted. For $K > 0$, we wish ξ to have positive and negative signs (to cover the full ξ path for evaluating ξ phase integrals in Fig. 1 and in Fig. 3 below) and so restrict η to positive values in the second plot in Fig. 1. For $K < 0$, to have η both positive and negative, ξ is restricted in the second plot in Fig. 2 to positive values. (The case of $K = 0$ is treated later.) The action variables J_ξ and J_η are functions of K and E via the phase–integral expressions:

$$J_\xi = \oint p_\xi(\xi)d\xi \ , \quad J_\eta = \oint p_\eta(\eta)d\eta \ , \tag{2.9}$$

where p_ξ and p_η are given by (2.7)–(2.8), and the integrals are over one cycle of ξ motion and of η motion, respectively. The above "change" in coordinate system, i.e., setting $\eta > 0$ and $-\infty < \xi < \infty$ when $K > 0$ and $-\infty < \eta < \infty$ and $\xi > 0$ when $K < 0$, has no effect on the quantization, which depends only on the topological properties of the trajectories, of the regions swept out, and of their caustics. The phase integral $\oint (p_x\,dx + p_y\,dy)$ along any path is invariant to any canonical transformation.

When $K > 0$, as in Figs. 1 and later in 3, the integral for J_ξ is the cyclic integral over ξ between $-c$ and c; the
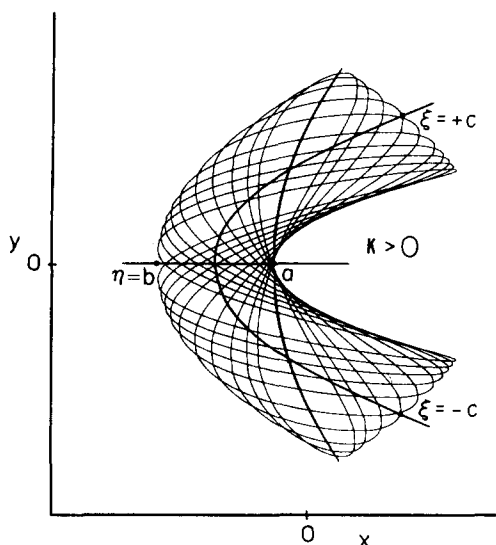
FIG. 3. Family of trajectories for the unperturbed problem with $K > 0$ (cf. Fig. 1). Along the curve of $\eta = $ constant ξ varies from a turning point at $\xi = -c$ to one at $\xi = +c$. Along the y axis ξ is constant ($= 0$) and η varies from a to b. Along the caustic passing through $\eta = a$, ξ equals a, and along the one passing through $\eta = b$, η equals b. In one trajectory the figure-eight has degenerated with a simple arc.

integral for J_η in (2.9) equals the cyclic integral over η between a and b in Figs. 1 and 3. When $K < 0$, as in Figs. 2 and later in 4, J_ξ is the cyclic ξ integral between a and b there, and J_η is the cyclic η integral between $-c$ and c. There is thus a discontinuity in the values of J_ξ and J_η when K passes through the value zero.

Each trajectory in the unperturbed $\omega_x = 2\omega_y$ resonant system is a closed curve, a distorted figure-eight. All trajectories in this unperturbed case are closed because of the commensurability of the unperturbed frequencies. We consider first an ensemble of unperturbed trajec-
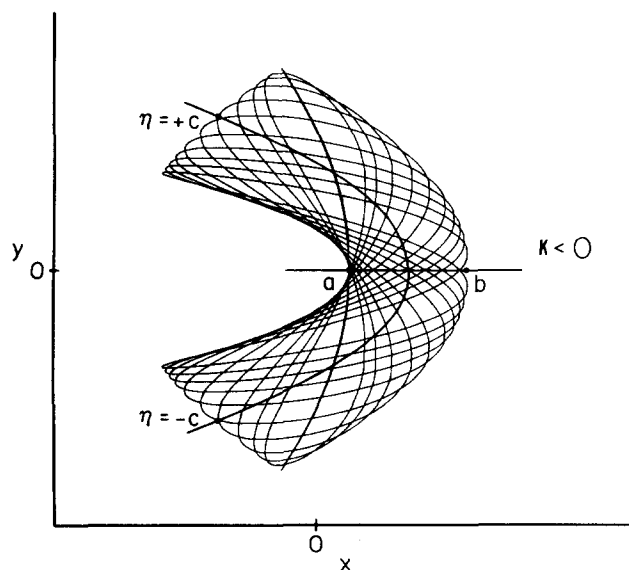

FIG. 4. Family of trajectories for the unperturbed problem with $K > 0$ (cf. Fig. 2). In Fig. 3, the legend with ξ and η are interchanged.
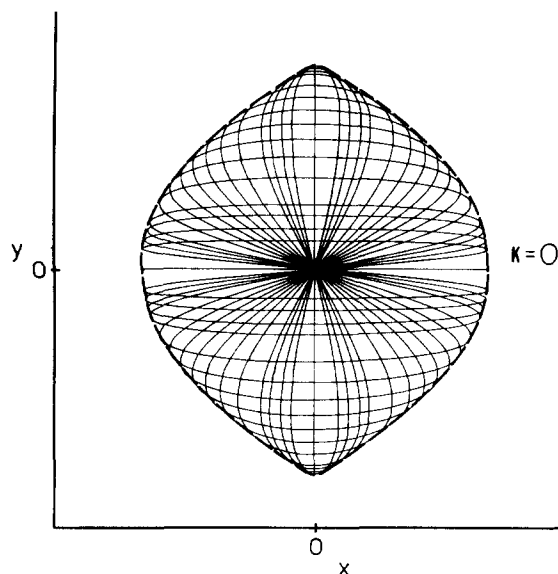

FIG. 5. Family of trajectories for which $K = 0$ for the unperturbed problem.

tories, each of which has the same J_ξ and the same J_η and hence the same K and E, but differs in the other initial constants and hence differs in initial phase. With this ensemble one obtains figures such as Fig. 3 for $K > 0$, Fig. 4 for $K < 0$, and Fig. 5 for $K = 0$.[9] In any one figure each closed figure-eight curve within a family is a single trajectory.

The quantization conditions are obtained as follows: Consider first a path along a single figure-eight trajectory in Figs. 3 to 5. In each of the cases $K > 0$ and $K < 0$, a trajectory touches a caustic six times during one figure-eight cycle. There is a semiclassical phase loss of $\pi/2$ each time the trajectory touches a caustic.[10] J, the phase integral $\oint_{\text{traj}} (p_x \, dx + p_y \, dy)$ along the closed trajectory, minus this phase loss of 3π, must equal $2\pi n$, where n an integer, in order that the semiclassical wave function be single valued. Thus, J is given by

$$J \equiv \oint_{\text{traj}} (p_x \, dx + p_y \, dy) = 2\pi(n + \tfrac{3}{2}) , \qquad (2.10)$$

where $n = 0, 1, 2, \ldots$. This quantization condition also applies to the figure-eight cycle when $K = 0$: Here, the trajectory touches the caustics in Fig. 5 four times, with a resulting phase loss of 2π, and passes through a focus once, with an additional phase loss[10] of π. One thus again obtains (2.10). Using Cartesian coordinates one can readily show that E depends only on n in the unperturbed case and that the degeneracy of the unperturbed system for any n is $(n/2) + 1$ or $(n + 1)/2$, according as n is even or odd, respectively (Appendix A).

Because of an invariance of $\Sigma_i \, p_i dq_i$ to a canonical transformation, the J in (2.10) is also given by

$$J = \oint_{\text{traj}} (p_\xi d\xi + p_\eta d\eta) , \qquad (2.11)$$

evaluated over one cycle of the figure-eight trajectory.

In addition to (2.10) a second quantization condition is needed. As in previous papers,[4,5] Poincaré surface of
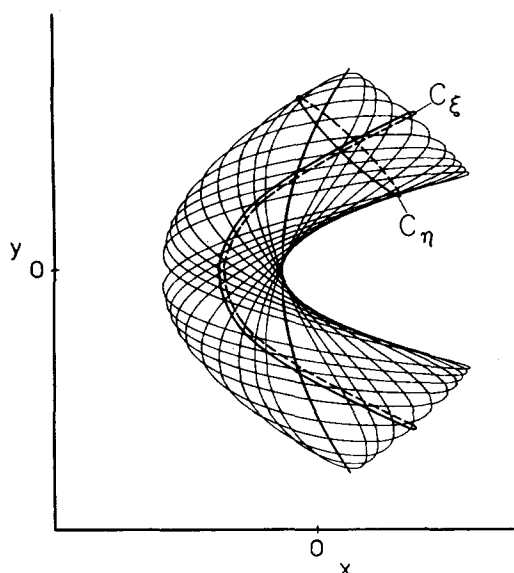
FIG. 6. The two independent path integrals for the unperturbed problem, for $K > 0$, are evaluated along the cited paths.

sections are introduced, curvilinear in the present case, one of constant η and one of constant ξ. On a $\eta = $ constant surface of section the integration path is indicated by the curve C_ξ in Fig. 6 for $K > 0$. Along this path the phase change in a semiclassical wave function is J_ξ minus π, since the phase loss at each of the two turning points is $\pi/2$. The net phase change must equal, for single valuedness of the semiclassical wave function, $2\pi n_\xi$, where n_ξ is an integer. Thus,

$$J_\xi = \oint p_\xi d\xi = 2\pi(n_\xi + \tfrac{1}{2}) \quad (K > 0, \eta = \text{constant}) , \quad (2.12)$$

where $n_\xi = 0, 1, 2, \ldots$. Similarly, when $K > 0$, the quantization condition for the η motion along a $\xi = $ constant path C_η in Fig. 6 is

$$J_\eta = \oint p_\eta d\eta = 2\pi(n_\eta + \tfrac{1}{2}) \quad (K > 0, \xi = \text{constant}) , \quad (2.13)$$

where $n_\eta = 0, 1, 2, \ldots$. Because there are two η cycles and one ξ cycle in a figure-eight trajectory in Fig. 6, the n in (2.10)–(2.11) can also be written as

$$n = 2n_\eta + n_\xi \quad (K > 0) . \quad (2.14)$$

When $K < 0$, the quantization condition is similarly derived, using Figs. 4 and 7 instead of Figs. 3 and 6. One obtains

$$J_\xi = \oint p_\xi d\xi = 2\pi(n_\xi + \tfrac{1}{2}) \quad (K < 0, \eta = \text{constant}) \quad (2.15)$$

$$J_\eta = \oint p_\eta d\eta = 2\pi(n_\eta + \tfrac{1}{2}) \quad (K < 0, \xi = \text{constant}) \quad (2.16)$$

$$n = 2n_\xi + n_\eta \quad (K < 0) . \quad (2.17)$$

In the case of $K = 0$ (Fig. 5), we have, by symmetry

$$J_\xi = J_\eta \quad (K = 0) \quad (2.18)$$

as the quantization condition, where J_ξ is defined as the $\oint p_\xi d\xi$ integral between $-c$ and c in Fig. 1 with $K = 0$,

and J_η is the $\oint p_\eta d\eta$ integral between $-c$ and c in Fig. 2 with $K = 0$.

Equations (2.10)–(2.18) will be used to quantize the system. In the unperturbed system the energy depends only on n. To characterize the states it will be useful to use the principal quantum number n and a quantum number l defined as follows:

$$l = n_\eta + 1 = (J_\eta/2\pi) + \tfrac{1}{2} \quad \text{if } K > 0 , \quad (2.19a)$$

$$= -(n_\xi + 1) = -(J_\xi/2\pi) - \tfrac{1}{2} \quad \text{if } K < 0 , \quad (2.19b)$$

$$= 0 \quad \text{if } K = 0 . \quad (2.19c)$$

The degeneracy is, we recall, $(n/2) + 1$ when n is even and $(n + 1)/2$ when n is odd. For any n, positive and negative values of l occur in pairs, and so the unpaired state $l = 0$ occurs only when the degeneracy is odd. The degeneracy is odd when n is an integer of the type $4N$ or $4N + 1$ $(N = 0, 1, 2, \ldots)$.

III. PERTURBED SYSTEM AND QUANTIZATION

In the perturbed system, a single trajectory sweeps out a region similar to that swept out by an ensemble of unperturbed trajectories in Figs. 3, 4, or 5. Examples are given in Figs. 8–10. When perturbed, a figure-eight trajectory of the type in Fig. 5 undergoes a "breathing" motion maintaining the focus near the origin, and so covers a region of shape similar to that of the ensemble of trajectories in Fig. 5, as in Fig. 10.

The quantum conditions in Sec. II apply to the perturbed case, as well as to the unperturbed one, with a modification of terminology: The constant K was a separation constant and so no longer describes the perturbed system. However, the cases of $K > 0$, $K < 0$, and $K = 0$ correspond to trajectory regions shaped as in Figs. 3, 4, and 5, respectively, and we shall continue to use this K terminology to describe similarly shaped figures for the perturbed system.
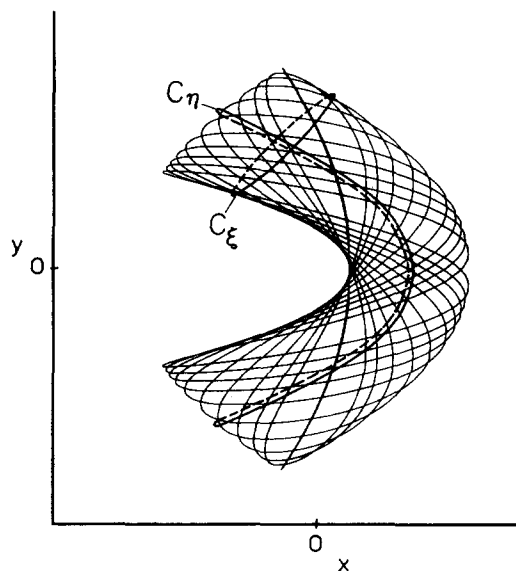

FIG. 7. The two independent path integrals for the unperturbed problem, for $K < 0$, are evaluated along the cited paths.
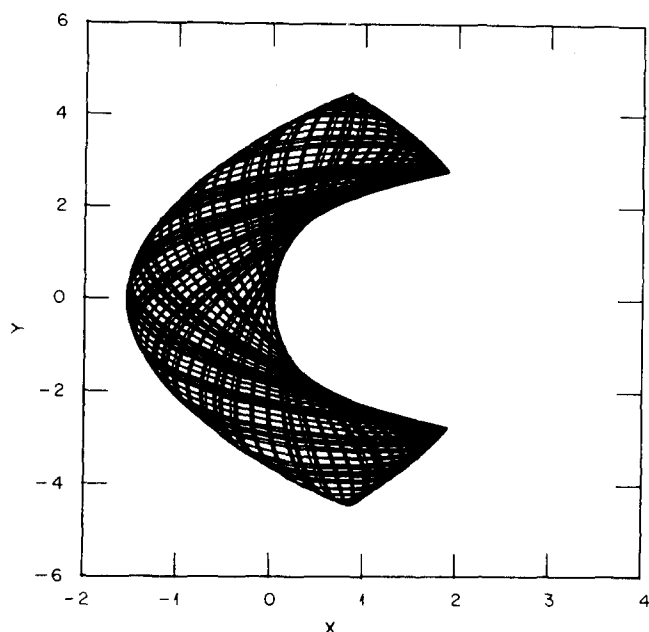
FIG. 8.   A $K > 0$ trajectory for the Hamiltonian (1.1) with $\omega_x = 1.4$, $\omega_y = 0.7$, $\lambda = -0.08$, $\alpha = 0.08$, $E = 4.265$, $x_0 = 0.038$.

To treat trajectories of the type in Figs. 3 and 4 (i.e., $K > 0$ and $K < 0$), we introduce curvilinear surfaces of section, as in Ref. 5 but now one of constant η and the other of constant ξ. An example of a perturbed trajectory of the type which generates a pattern similar to Fig. 3 is given in Fig. 8. Figure 8 is described by a
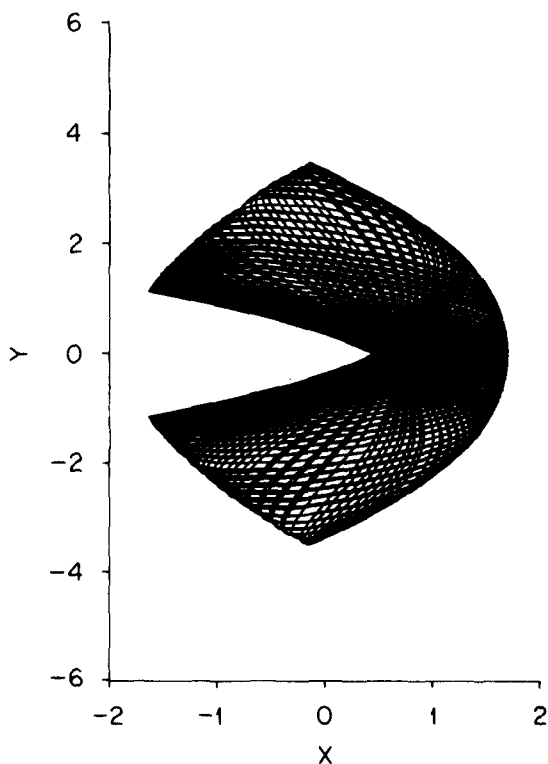

FIG. 9.   A $K < 0$ trajectory for the Hamiltonian (1.1), one with a cusplike caustic, with $\omega_x = 1.4$, $\omega_y = 0.7$, $\lambda = -0.08$, $\alpha = 0.08$, $E = 31.50$, $X_0 = 0.065$.
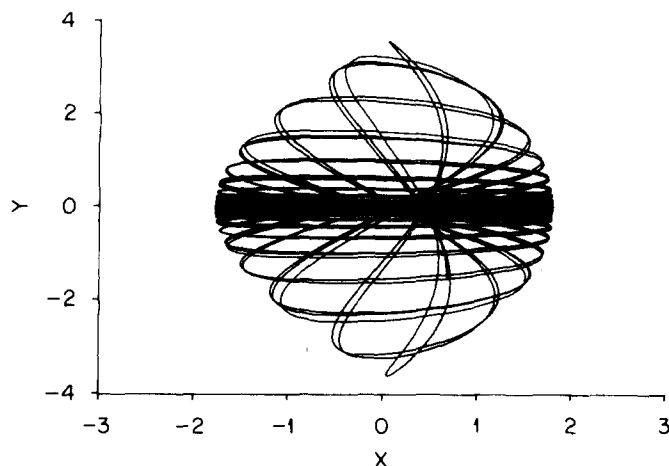

FIG. 10.   A $K = 0$ trajectory for the Hamiltonian (1.1), with $\omega_x = 1.4$, $\omega_y = 0.7$, $\lambda = -0.08$, $\alpha = 0.08$, $E = 3.150$, $p_y = \sqrt{2E}$. ($p_x = x = y = 0$).

single trajectory, a librating figure-eight trajectory, whereas Fig. 3 was described by a family of trajectories. A curvilinear surface of section at a given η, corresponding to the C_ξ path which cuts the same two caustics as Fig. 6, yields a p_ξ vs ξ of the form in Fig. 11. J_ξ can be calculated from the area of the p_ξ vs ξ curve, using (2.9).

Similarly, a plot of p_η vs η for a curve of constant ξ can be obtained corresponding to any path equivalent to C_η in Fig. 6. Here, the value of the phase integral J_η along any C_η in Fig. 6 equals that of the phase integral $\int p_x \, dx$ along a $y = 0$ Cartesian surface of section.[11] A plot of p_x vs x is given in Fig. 12. Equation (2.13) becomes
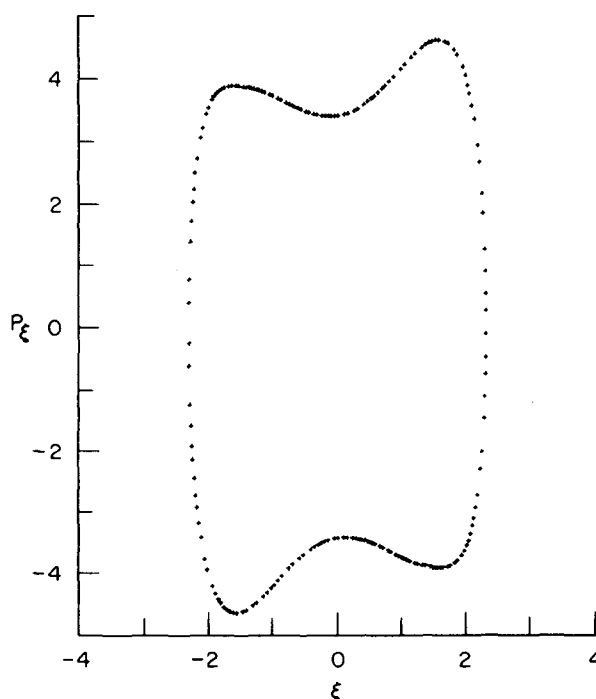

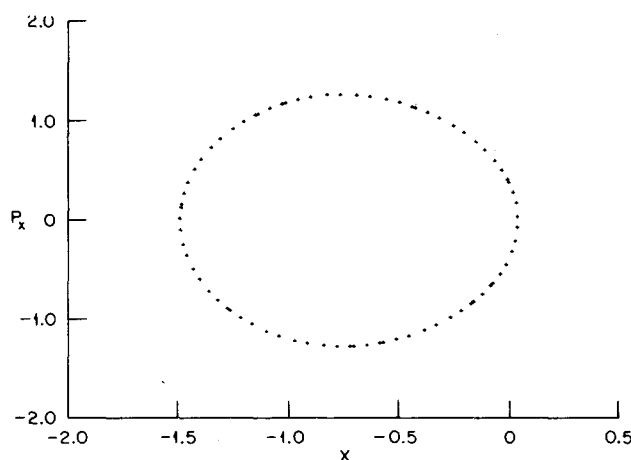FIG. 11.   The $\eta = 1.7$ surface of section for the trajectory in Fig. 8.

FIG. 12.   The $y = 0$ surface of section for the trajectory in Fig. 8.

$$\oint p_x \, dx = J_\eta = 2\pi(n_\eta + \tfrac{1}{2}) \ . \tag{3.1}$$

The quantum conditions actually imposed on a trajectory of the type in Fig. 8 were Eqs. (3.1) and (2.12). However, sometimes it was convenient (because of spacing of points) to use (2.13) instead of (3.1). Any of these conditions could have been equally well replaced by Eq. (2.10), utilizing the "close trajectory" method of Ref. 5. Once n_ξ and n_η, and hence n, is obtained l is calculated using (2.19a). Similar remarks apply to trajectories for the type similar to Fig. 4, but with the roles of ξ and η reversed. Numerical calculations verified that the value of J_η obtained from (3.1) was the same as that obtained from (2.13) using Poincaré surfaces of section of constant ξ along other values of $\xi = $ constant, as indeed it should be.

To use the quantum conditions of Sec. II for trajectories of the type in Fig. 5 we employ Eqs. (2.10) and (2.18). To a high degree of approximation the trajectory closes itself at the focus or at a "near focus," after each single figure-eight cycle as in Fig. 10. This $K = 0$ case arises only for $n = 4N$ and $n = 4N + 1$, as discussed in Sec. II. The actual integration of (2.10) was done by

TABLE I.   Eigenvalues for the case where $\omega_x = 2\omega_y$ in the Hamiltonian (1.1).[a]

State (n, l)	E^0	E_{quantum}	E_{semi}
(0, 0)	1.050	1.048	1.050
(1, 0)	1.750	1.739	1.750
(2, +1)	2.450	2.384	2.388
(2, −1)	2.450	2.485	2.476
(3, +1)	3.150	3.028	3.028
(3, −1)	3.150	3.204	3.207
(4, +1)	3.850	3.653	3.654
(4, 0)	3.850	3.825	3.840
(4, −1)	3.850	3.945	3.941
(5, +1)	4.550	4.265	4.265
(5, 0)	4.550	4.490	4.550
(5, −1)	4.550	4.682	4.682

[a] $\omega_x = 1.4$, $\omega_y = 0.7$, $\lambda = -0.08$, $\alpha = 0.08$.

TABLE II.   Eigenvalues for the case where $\omega_x = 2\omega_y$ in the Hamiltonian (1.1).[a]

State (n, l)	E^0	E_{quantum}	E_{semi}
(0, 0)	1.050	1.050	1.050
(1, 0)	1.750	1.747	1.750
(2, +1)	2.450	2.442	2.421
(2, −1)	2.450	2.471	2.467
(3, +1)	3.150	3.100	3.099
(3, −1)	3.150	3.184	3.185
(4, +1)	3.850	3.769	3.769
(4, 0)	3.850	3.844	3.850
(4, −1)	3.850	3.906	3.908
(5, +1)	4.550	4.434	4.434
(5, 0)	4.550	4.536	4.549
(5, −1)	4.550	4.631	4.630
(6, +2)	5.250	5.095	5.093
(6, +1)	5.250	5.204	5.205
(6, −1)	5.250	5.268	5.261
(6, −2)	5.250	5.358	5.358

[a] $\omega_x = 1.4$, $\omega_y = 0.7$, $\lambda = -0.04$, $\alpha = 0.04$.

introducing an additional differential equation [Eq. (3.2)] and integrating the latter along the trajectory

$$J = \int_0^T (p_x \dot{x} + p_y \dot{y}) dt \ , \tag{3.2}$$

where T is the time for the trajectory to undergo the cycle in the close trajectory method of Ref. 5.

Systems with negative l had trajectory-covered regions similar to Fig. 4, those with positive l similar to Fig. 3 and those with $l = 0$ similar to Fig. 5.

In the case of trajectories sweeping out regions similar to that in Fig. 4, cusps were sometimes obtained near the y axis, as in Fig. 9, but caused no difficulty and no need to alter the foregoing procedure.

IV. RESULTS

A. Eigenvalues

The initial conditions for a trajectory involved the specification of E, the initial x, x_0, and the setting of the initial $p_x = y = 0$; the initial $|p_y|$ was then chosen to yield the specified energy E. For any trajectory it was always possible to choose $p_x = 0$ and $y = 0$, since such a choice corresponds to an end-point of the x motion in the Poincaré surface of section $y = 0$. The surface of section data was obtained from a trajectory using a linear interpolation on both sides of the surface.[12]

In the case of the transitional type trajectory, the $K = 0$ trajectory (e.g., Fig. 10), the system spends a lot of time on or near the y axis. Accordingly, such trajectories were readily generated by choosing $x_0 = y_0 = 0$ and making the p_y very close to zero; p_x was then chosen to yield the specified energy. For the reason discussed earlier, such trajectories were sought only for $n = 4N$ and $n = 4N + 1$, $N = 0, 1, 2, \ldots$. The results for the 1:2 resonance are tabulated in Tables I and II, which give

TABLE III. Eigenvalues for the case where $\omega_x = \frac{1}{2}\omega_y$ in the Hamiltonian (1.1).[b]

State (n_x, n_y)	E^0	$E_{quantum}$	E_{semi}
0, 0	1.050	1.048	1 048
1, 0	1.750	1.744	1.744
2, 0	2.450	2.439	2.439
0, 1	2.450	2.439	2.438
3, 0	3.150	3.130	3.130
1, 1	3.150	3.135	3.132

[a]$\omega_x = 0.7$, $\omega_y = 1.4$, $\lambda = -0.08$, $\alpha = 0.08$.

the quantum numbers n and l, the unperturbed energy E_0, the quantum mechanical energy and the semiclassical value. The semiclassical eigenvalues are linear interpolations of three trajectories which had n_ξ and n_η values which were close to the desired integers.

The quantum mechanical calculations required a larger Cartesian basis set than that used in the previous[4,5] systems: Usually 49 elements sufficed previously, but now 64 and even 100 were needed. For example, one eigenvalue calculated was 4.282 with a basis set of 49 elements. It changed to 4.265 for 64 elements and remained the same for 100 elements. A basis set based on separation in parabolic coordinates would be useful, if the matrix elements could be evaluated analytically.

Some trajectories were also obtained for the $\omega_y = 2\omega_x$ case. They were boxlike rather than paraboliclike. Their treatment is the same as that for the boxlike trajectories in Ref. 4. In the quantum mechanical calculations a basis set of 49 elements sufficed. Results for this 2:1 resonance are given in Table III.

B. Quantum mechanical wave functions

For further comparison of the classical and quantum behavior, wave functions were computed from the variational calculations, and the features were compared with the regions swept out by the revelant trajectories. Calculations were made for the quasiperiodic regions, to which the considerations of Sec. II and III apply, and for
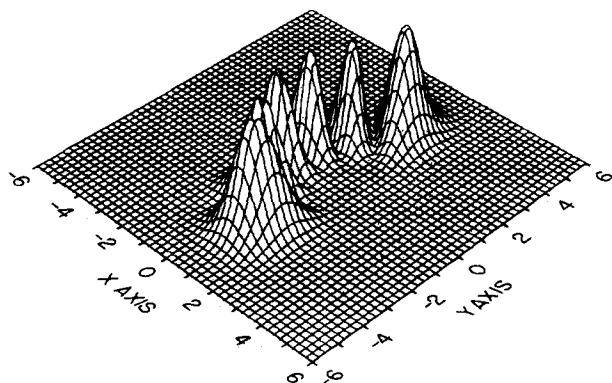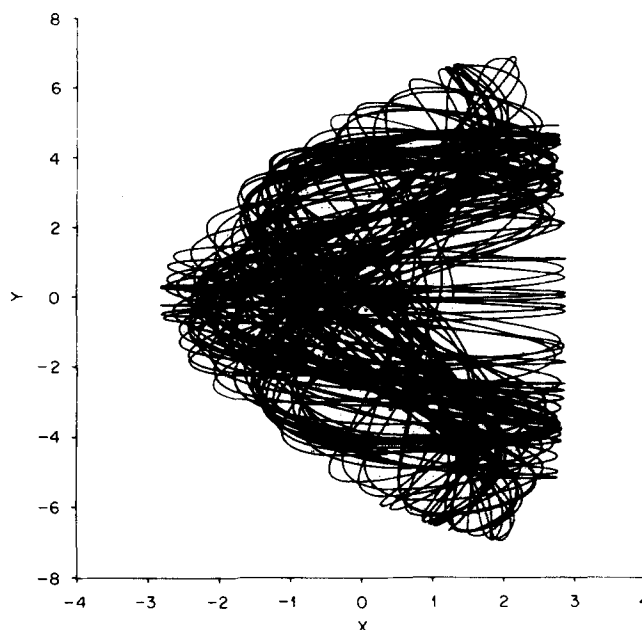

FIG. 14. A trajectory for the Hamiltonian (1.1) in the ergodic region, with $\omega_x = 1.4$, $\omega_y = 0.7$, $\lambda = -0.08$, $\alpha = 0.08$, $E = 8.0$ $x_0 = 1.3$.

the stochastic regime, for which those semiclassical considerations do not apply. A wave function from the energy region where the eigentrajectory (a trajectory which corresponds to the eigenvalue) was of the type in Fig. 8 is shown in Fig. 13. The trajectory occupies a curved region of coordinate space and the wave function is oscillatory within this region, being a damped exponential outside even though it is still within the energetically allowed region. When the motion is stochastic, the trajectory (Fig. 14) is seen to occupy the entire energetically allowed region of coordinate space and the wave function (Fig. 15) is oscillatory over the entire classically allowed coordinate space and a damped exponential in the forbidden region. In the high energy ("stochastic") region we found several quanperiodic trajectories and their analogous quantum mechanical wave functions.

Another interesting aspect of the motion in the quasi-

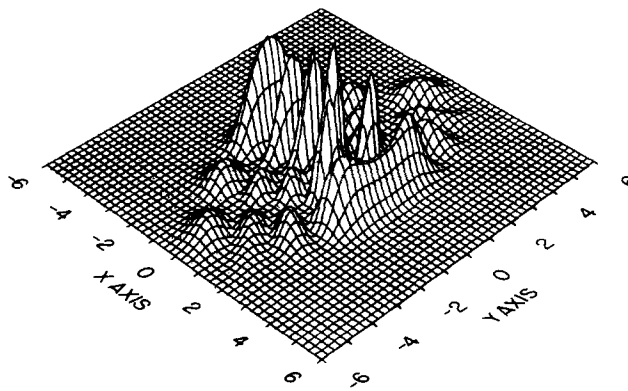FIG. 13. A wave function in the quasiperiodic region, corresponding to the trajectory in Fig. 8.

FIG. 15. A wave function in the ergodic region, corresponding to the trajectory in Fig. 14.

periodic regime is that the present system is seen to exhibit an extensive periodic energy sharing between the x and y normal modes (e.g., Figs. 8–10). This is a dramatic example of the breakdown of the normal mode approach even in the quasiperiodic region.

C. Stochastic limit considerations

Inasmuch as the considerations of Sec. II and III apply only to the quasiperiodic regime it is useful to examine several approaches which have been used to predict the stochastic limit.

At energies above $E \cong 7$ for the present λ and α, the trajectories begin to fill the energetically accessible coordinate and phase space (become stochastic). In the example given in Fig. 14, the system is seen to occupy all of the energetically accessible region unlike the trajectories in Figs. 8–10. The changes in shape of the figure-eight cycles show that J_ξ and J_η are no longer constants of the motion. Indeed, only the energy is the "constant" of a sufficiently long-time trajectory, in the stochastic system, since all parts of the energetically accessible phase space are covered. There are significant similarities between the classical stochastic system in Fig. 14 and the corresponding stochastic quantum mechanical one in Fig. 15. The shape of the regions covered is similar (the energetically accessible space); the region of greatest probability in Fig. 15 corresponds to that of the densest number of trajectories in Fig. 14.

Various approaches have been developed to obtain the stochastic limit, i.e., to obtain the energy below which the system is largely quasiperiodic and above which it is largely stochastic. One of these methods is that of overlapping resonances, due to Chirikov.[12] Several applications of it have been made in the literature.[13] However it cannot be applied, at least not in a simple form, to the present problem because there are no first order resonances other than the 1:2 resonance, and so no overlapping of resonances.

Another method for obtaining the stochastic limit is that due to Toda,[14] with a similar equation for the limit having been obtained also by Brumer.[14] This second method has worked reasonably well for a couple of systems.[14] However, it has been shown to fail as a global criterion.[15,16] We illustrate its application to the present system here and see that at least in the neighborhood of $\alpha = -2$ it breaks down.

The method uses the exponential separation of trajectories as a criterion of stochasticity, and uses an approximation to see when the separation is exponential. The calculation involves forming a differential equation for the separation in x space, Δx, and also for Δy, of two adjacent trajectories, linearizing that equation if necessary, and then solving for the behavior of $\Delta x(t)$ and $\Delta y(t)$. Second derivatives for a two-coordinate system are,

$$r = \partial^2 V/\partial x^2 , \qquad t = \partial^2 V/\partial y^2 , \qquad s = \partial^2 V/\partial x \partial y . \qquad (4.1)$$

It is concluded that the motion will be stochastic when
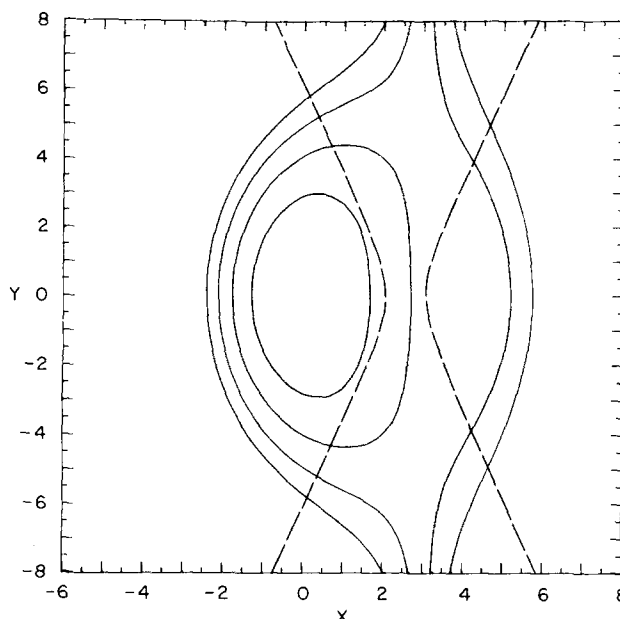
$$rt - s^2 < 0 . \qquad (4.2)$$

FIG. 16. The contour of (4.3) (dashed lines) is superimposed on the potential energy contours (solid lines) for $E = 2$, 4, 6, and 8.

In the present case, with the $V(x, y)$ from Eq. (1.1) one finds that

$$rt - s^2 = (\omega_x^2 - 6\lambda\alpha x)(\omega_y^2 + 2\lambda x) - 4\lambda^2 y^2 = 0 . \qquad (4.3)$$

Setting $rt - s^2 = 0$ is intended to yield the stochastic limit. However, for $\alpha = -2$ the perturbed system is separable in parabolic coordinates, since the Hamiltonian for $\alpha = -2$ is

$$H = [\tfrac{1}{2}(p_\xi^2 + p_\eta^2 + \xi^6 + \eta^6) + \lambda/4(\xi^8 - \eta^8)] \, 1/(\xi^2 + \eta^2), \qquad (4.4)$$

and so by setting $H = E$ one sees that on multiplying by $\xi^2 + \eta^2$ one can separate (4.4) into two equations. Therefore, this system cannot exhibit stochastic behavior at any energy. Figure 16 shows the contour of Eq. (4.3) superimposed on the potential energy surface with $\alpha = -2$ and $\lambda = -0.08$, thus predicting regions of stochasticity. This result suggests that this prediction of a local instability is not a sufficient criterion of stochastic behavior for bound state or scattering problems.

V. DISCUSSION

A comparison of the $\omega_x = 2\omega_y$ and $\omega_y = 2\omega_x$ cases shows that the effect of the perturbation is considerably larger in the former, as expected.

The quantum and semiclassical results for the $\omega_x = 2\omega_y$ system, compared in Tables I and II, are seen to agree moderately well. The agreement for the $\omega_y = 2\omega_x$ (Table III) is quite good. In the $\omega_x = 2\omega_y$ case a large rather periodic energy-sharing between the x and y motions usually occurs—in some cases the figure-eight motion is largely in the x direction and sometimes largely in the y direction. The system for $\alpha \cong -2$, is separable and provides an example where the simple stochastic limit considerations of Ref. 14 break down.

It is interesting to note the various types of caustics, which depend on the initial conditions for a given E.

For example, for some x_0, the region swept out by a trajectory is as in Fig. 8, without a cusp. Here, a figure-eight cycle touches the caustics six times, for a total phase loss of 3π. A variation of x_0 introduces a cusp, as in Fig. 9. The cusp serves as a focus for some of the figure-eight cycles, namely those which touch the inner caustics twice during a cycle and the outer caustic twice. The total loss of phase due to touching the caustic and passing through a focus is 3π per figure-eight cycle.

The wave functions in the quasiperiodic regime occupy localized regions of coordinate space corresponding to the trajectory (as in Fig. 13), and in the stochastic regime the entire classically allowed region (as in Fig. 15).

In the quasiperiodic region the energy in a given "mode" fluctuates periodically while in the ergodic region it fluctuates more "randomly." We are currently investigating the behavior of the mode energy autocorrelation function in the two regions.

ACKNOWLEDGMENT

APPENDIX A. DEGENERACY AND OTHER PROPERTIES OF THE UNPERTURBED SYSTEM

We let J_x and J_y denote the unperturbed action variables and w_x and w_y the conjugate angles. The Cartesian coordinates and momenta are then[7]

$$x = (J_x/\pi\omega_x)^{1/2}\sin 2\pi w_x ,$$
$$p_x = (J_x\omega_x/\pi)^{1/2}\cos 2\pi w_x , \tag{A1}$$

with analogous equations for y and p_y.

For system with a given J_x and J_y, a single trajectory sweeps out a region covered by a rectangular box, when ω_x and ω_y are incommensurate, with amplitudes in the x and y directions equal to $(J_x/\pi\omega_x)^{1/2}$ and $(J_y/\pi\omega_y)^{1/2}$, respectively.

Along any figure-eight trajectory the unperturbed system has one cycle of the y motion and two of the x motion when $\omega_x = 2\omega_y$. Thus, the total phase integral J along this trajectory is

$$J \equiv \oint_{\text{traj}} (p_x\,dx + p_y\,dy) = 2J_x + J_y . \tag{A2}$$

The unperturbed energy of the two oscillators equals[7] $(J_x\omega_x + J_y\omega_y)/2\pi$, and so equals $J/2\pi$, since $\omega_x = 2$ and $\omega_y = 1$. It thus depends only on J. The quantization conditions for the unperturbed oscillator are

$$J_x = 2\pi(n_x + \tfrac{1}{2}) , \qquad J_y = 2\pi(n_y + \tfrac{1}{2}) \tag{A3}$$

in units of $\hbar = 1$, with n_x, $n_y = 0, 1, 2, \ldots$. Thus, the J in (A1) equals

$$J = 2\pi(n + \tfrac{3}{2}) , \tag{A4}$$

where

$$n = 2n_x + n_y , \qquad n = 0, 1, 2, \ldots . \tag{A5}$$

For any n the degeneracy is seen from (A5) to be $(n/2) + 1$ or $(n+1)/2$, for n even or odd, respectively. Also, since E depends only on J it depends only on n [cf. (A2)]. The degeneracy is unchanged, of course, if one quantizes J_ξ and J_η instead of J_x and J_y.

In these action-angle coordinates the perturbed Hamiltonian (1.1) is

$$H = \omega_x J_x + \omega_y J_y - \lambda(J_x/\pi\omega_y)^{1/2}(J_y/4\pi\omega_y)[\sin 2\pi(w_x + 2w_y)$$
$$+ \sin 2\pi(w_x - 2w_y) - 2\sin 2\pi w_x] - \lambda\alpha(J_x/\pi\omega_x)^{3/2}\sin^3 2\pi w_x , \tag{A6}$$

thus yielding the secular perturbation term discussed in the text.

[1] E.g., H. C. Allen and P. C. Cross, *Molecular Vib-Rotors* (Wiley, New York, 1963); E. Fermi, Z. Phys. **71**, 250 (1931); Y. Morino and S. Saito, J. Mol. Spectrosc. **19**, 435 (1966); I. Suzuki, *ibid*. **25**, 479 (1968); V. E. Bondybey and S. H. English, J. Chem. Phys. **67**, 2868 (1977).

[2] R. A. Marcus, Discuss. Faraday Soc. **55**, 34 (1973).

[3] W. Eastes and R. A. Marcus, J. Chem. Phys. **61**, 4301 (1974).

[4] D. W. Noid and R. A. Marcus, J. Chem. Phys. **62**, 2119 (1975).

[5] (a) D. W. Noid and R. A. Marcus, J. Chem. Phys. **67**, 559 (1977); (b) cf. D. W. Noid, Ph.D. Thesis, University of Illinois, Urbana (April 1976) [D. W. Noid, Diss. Abstr. Int. B **37**, 2278 (1967)].

[6] (a) L. C. Percival and N. Pomphrey, Mol. Phys. **31**, 917 (1976); S. Chapman, B. Garrett, and W. H. Miller, J. Chem. Phys. **64**, 502 (1976); K. S. Sorbie and N. C. Handy, Mol. Phys. **32**, 1327 (1976); K. S. Sorbie, *ibid*. **32**, 1577 (1976); N. C. Handy, S. M. Colwell, and W. H. Miller, Faraday Discuss. Chem. Soc. **62**, 29 (1977); I. C. Percival, Adv. Chem. Phys. **36**, 1 (1977); K. S. Sorbie and N. C. Handy, Mol. Phys. **33**, 1319 (1977); J. B. Delos and R. T. Swimm, Chem. Phys. Lett. **47**, 76 (1977); R. T. Swimm and J. B. Delos, Chem. Phys. Lett. (in press); (b) R. T. Swimm, Ph.D. Thesis, University of William and Mary, 1978.

[7] M. Born, *Mechanics of the Atom* (Ungar, New York, 1960).

[8] A parabolic coordinate system is given in P. M. Morse and H. Feshbach, *Methods of Theoretical Physics* (McGraw-Hill, New York, 1953), Vol. 1, p. 501. The curves of constant ξ are confocal parabolas, with axes along the x axis and open to the left. The one with $\xi = 0$ shrinks to the negative x axis. The curves of constant η are orthogonal to the previous family, and are confocal parabolas with axes along the x axis but open-ended to the right. The curve with $\eta = 0$ shrinks to the positive x axis. (Fig. 5.1. of the above reference.)

[9] In Fig. 5, where $K = 0$, the right hand curved boundary is $\xi = c = a$, in the case of the $K > 0$ convention on signs of ξ and η, and $\xi = c = a$ for $y < 0$, $\xi = -c = -a$ for $y < 0$ in the case of the $K < 0$ convention on signs. Analogous remarks regarding η apply to the left hand curved boundary.

[10] E.g., J. B. Keller, Ann. Phys. (N.Y.) **4**, 180 (1958).

[11] The numerical integration was done using the Simpson Rule Method for for unequally spaced points as discussed in Ref. 4. The trajectory was integrated with SSP routine DHPCG on the IBM 360/91 computer.

[12] B. V. Chirikov, *Research Concerning the Theory of Nonlinear Resonance and Stochasticity* (Report No. 267, Institute of Nuclear Physics, Novosibirsk, U.S.S.R., 1969), [Transl. 17-40 CERN, Geneva, 1971); B. V. Chirikov, E. Keil, and A.

M. Sessler, J. Stat. Phys. **3**, 307 (1971); J. Ford and G. H. Lunsford, Phys. Rev. A **1**, 59 (1970).

[13]M. A. Lieberman and A. J. Lichtenberg, Phys. Rev. A **5**, 1852 (1972); E. F. Jaeger and A. J. Lichtenberg, Ann. Phys. **71**, 319 (1972); Ref. 5b; Chap. 8; D. W. Oxtoby and S. A. Rice, J. Chem. Phys. **65**, 1676 (1976); M. L. Koszykowski, Ph. D. Thesis, University of Illinois, 1978.

[14]M. Toda, Phys. Lett. A **48**, 335 (1974); cf. P. Brumer and

J. W. Duff, J. Chem. Phys. **65**, 3566 (1976); *ibid*. **67**, 4898 (1977). Analogous equations were developed for a stability problem different from stochasticity of anharmonically coupled vibrations in P. Brumer, J. Comput. Phys. **14**, 391 (1973).

[15]G. Benettin, R. Brambilla, and L. Calgani, Phys. Rev. A **87**, 381 (1977).

[16]G. Casati, Lett. Nuovo Cimento **14**, 311 (1975); G. Casati and J. Ford, Phys. Rev. A **12**, 1702 (1975).